GRK6 depletion induces HIF activity in lung adenocarcinoma

Sumei Yao[1,7], Ayse Ertay[2,7], Yilu Zhou[2,3,7], Liudi Yao[2], Charlotte Hill[2], Jinliang Chen[1], Yangbo Guan[4], Hui Sun[5], Rob M. Ewing[2,3], Yifei Liu[5,6,*], Xuedong Lv[1,*], and Yihua Wang[2,3,*]

[1]Department of Respiratory Medicine, The Second Affiliated Hospital of Nantong University, Nantong 226001, People's Republic of China.

[2]Biological Sciences, Faculty of Environmental and Life Sciences, University of Southampton, Southampton SO17 1BJ, UK.

[3]Institute for Life Sciences, University of Southampton, Southampton SO17 1BJ, UK.

[4]Department of Urology, Affiliated Hospital of Nantong University, Nantong 226001, People's Republic of China.

[5]Department of Pathology, Affiliated Hospital of Nantong University, Nantong 226001, People's Republic of China.

[6]Medical School of Nantong University, Nantong 226001, People's Republic of China.

[7]These authors contributed equally to this work

*** Correspondence:**
Yifei Liu (ntdxliuyifei@sina.com)

Xuedong Lv (email: lvxuedong1968@163.com)

Yihua Wang (e-mail: yihua.wang@soton.ac.uk)

Keywords: GRK6, HIF, lung adenocarcinoma, hypoxia, EMT

Abstract

G protein-coupled receptor kinase 6 (GRK6) is expressed in various tissues and is involved in the development of several diseases including lung cancer. We previously reported that GRK6 is down-regulated in lung adenocarcinoma patients, which induces cell invasion and metastasis. However, further understanding of the role of GRK6 in lung adenocarcinoma is required. Here we explored the functional consequence of *GRK6* inhibition in lung epithelial cells. Analysis of TCGA data was coupled with RNA sequencing (RNA-seq) in alveolar epithelial type II (ATII) cells following depletion of *GRK6* with RNA interference (RNAi). Findings were validated in ATII cells followed by tissue microarray analysis. Pathway analysis suggested that one of the Hallmark pathways enriched upon GRK6 inhibition is 'Hallmark_Hypoxia' (FDR = 0.014). We demonstrated that *GRK6* depletion induces HIF1α (hypoxia-inducible factor 1 alpha) levels and activity in ATII cells. The findings were further confirmed in lung adenocarcinoma samples, in which GRK6 expression levels negatively and positively correlate with HIF1α expression ($P = 0.015$) and VHL expression ($P < 0.0001$), respectively. Mechanistically, we showed the impact of GRK6 on HIF activity could be achieved via regulation of VHL levels. Taken together, targeting the HIF pathway may provide new strategies for therapy in GRK6-depleted lung adenocarcinoma patients.

1 Introduction

G protein-coupled receptor kinases (GRKs) are a family of kinases that play a critical role in G protein-coupled receptors (GPCRs) homologous desensitization. GRKs phosphorylate specific serine and threonine residues of activated GPCRs which promote high affinity binding of arrestins and then suppress further G protein activation by interrupting receptor-G protein coupling (Bouvier et al., 1988; Vroon et al., 2006; Raghuwanshi et al., 2013). Desensitization of GPCRs has a critical role in maintaining homeostasis. As such, abnormal GPCRs desensitization can cause a variety of human diseases, including autoimmune diseases (Balabanian et al., 2005), asthma (Wang et al., 2009), heart failure (Rockman et al., 1998), Parkinson's disease (Gainetdinov et al., 2003), inappropriate diuresis (Barak et al., 2001) and tumour progression and metastasis (Yu et al., 2018). Therefore, GRKs are important therapeutic targets for these diseases.

G protein-coupled receptor kinase 6 (GRK6) is a member of the GRK family, which is expressed in various tissues and involved in the development of several diseases (Willets et al., 2002; Ahmed et al., 2010; Tiedemann et al., 2010). High expression of GRK6 has been reported in hepatocellular carcinoma (Li, 2013), colorectal cancer (Tao et al., 2018); whilst lower expression was reported in hypopharyngeal squamous cell carcinoma (Qiu et al., 2016) compared to normal tissues. Further, *Grk6* knock out mice ($Grk6^{-/-}$) showed a significant increase in the growth and metastasis of Lewis lung cancer (LLC) compared to the control mice ($Grk6^{+/+}$) (Raghuwanshi et al., 2013). Our previous study suggested that GRK6 expression was significantly down-regulated in lung adenocarcinoma patients, and its level was an independent prognostic factor for overall survival (Yao et al., 2016). Moreover, we also showed that the promoter region of the *GRK6* gene was hyper-methylated in lung adenocarcinoma tissues compared to the normal tissue samples, leading to a down-regulation of *GRK6* expression and in turn, inducing cell invasion and metastasis (Yao et al., 2019b). However, further understanding of the role of GRK6 in lung adenocarcinoma is required.

In this study, we aimed to investigate the functional consequence of *GRK6* depletion in lung epithelial cells. Analysis of TCGA data was coupled with RNA sequencing (RNA-seq) in alveolar epithelial type II (ATII) cells following the depletion of *GRK6* with RNA interference (RNAi). Tissue microarrays were used to investigate the expression and function of *GRK6* in lung adenocarcinoma. Our data suggests that *GRK6* depletion induces HIF1α (hypoxia-inducible factor 1 alpha) activity. Targeting the HIF pathway may provide new strategies for therapy in GRK6-depleted lung adenocarcinoma patients.

2 Materials and Methods

2.1 Cell culture, transfections and reagents

ATII (alveolar epithelial type II, kindly provided by Prof Julian Downward, The Francis Crick Institute, UK) cells (Molina-Arcas et al., 2013; Coelho et al., 2017; Hill et al., 2019; Yao et al., 2019a) were cultured in DCCM-1 (Biological Industries Ltd) supplemented with 10% new-born calf serum (NBCS) (Life Technologies), 1% penicillin, 1% streptomycin, and 1% L-glutamine (all from Life Technologies). All cells were kept at 37 °C and 5% CO_2. No mycoplasma contamination was detected in the cell lines used.

Short interfering RNA (siRNA) oligos against *GRK6* or control siRNA were purchased from Biomics Biotechnologies Co., Ltd, China. Sequences were available from an earlier publication (Yao et al., 2019b). Cells were transfected with the indicated siRNA oligos at a final concentration of 35 nM using Dharmafect 2 reagent (Dharmacon).

2.2 RNA isolation, library construction, and sequencing

To identify global transcriptomic changes in ATII cells upon *GRK6* depletion, RNA sequencing (RNA-seq) was performed. In brief, ATII cells were transfected with either control siRNA or siRNA against *GRK6* for 3 days. Total RNA was isolated using an RNeasy mini kit (Qiagen) according to the manufacturer's instructions and quantified using a Nanodrop Spectrophotometer 2000c (Thermo Fisher Scientific). A total amount of 3 μg RNA per sample was used as input material for library construction. Sequencing libraries were generated using NEBNext® UltraTM RNA Library Prep Kit for Illumina® (NEB, Ipswich, Massachusetts, USA) following the manufacturer's instructions. Libraries were pooled in equimolar and sequenced using the paired-end strategy (2 × 150) on the Illumina NovaSeq 6000 platform following the standard protocols (Novogene, UK). RNA-seq data have been deposited in the Gene Expression Omnibus (GEO) database (accession code GSE164921).

2.3 RNA-seq data analysis

Quality control of RNA-seq data was performed using FastQC (http://www.bioinformatics.babraham.ac.uk/projects/fastqc) and MultiQC (Ewels et al., 2016). Trim Galore (https://github.com/FelixKrueger/TrimGalore) was used to trim adapters, reads with low quality (< 30), and short length (< 50 bp). RNA-seq reads were mapped to Human genome Ensembl GRCh38 using Hisat2 (Kim et al., 2015) (version 2.1.0) with default codes. Sam files were transformed into bam files using samtools (Li et al., 2009) (version 1.9). The read counts of each gene were summarized using featureCounts (Liao et al., 2014) (version 1.6.5). Raw read counts were imported into RStudio (version 3.6.1) and analysed by using R package of DESeq2 (Love et al., 2014) (version 1.26.0). Transcripts with low abundance (under 10 counts across all samples) were removed. Genes with a false discovery rate (FDR) *P*-value less than 0.05 adjusted by using Benjamini–Hochberg (BH) method (or q-value) were considered as differentially expressed genes (DEGs). Gene ontology (GO) enrichment analysis was generated through ToppGene (ToppGene Suite for gene list enrichment analysis and candidate gene prioritization) website (https://toppgene.cchmc.org/). Parameter was set as FDR < 0.05. All downstream analysis was performed in RStudio (version 3.4.4).

2.4 Data mining *GRK6* related data from the Cancer Genome Atlas (TCGA)

The expression of mRNAs in the TCGA lung adenocarcinoma (LUAD) (IlluminaHiSeq) dataset was obtained from the UCSC Xena Browser (https://xenabrowser.net/). To separate the low and high *GRK6* group in the TCGA dataset, hierarchical cluster was performed on the high correlated genes with GRK6 via Pearson analysis in RStudio (version 3.4.4). According to the correlation analysis, there were 17 samples in the high *GRK6* group and 26 samples in the low *GRK6* group. Then, an unpaired *t-test* was performed to identify significantly expressed mRNAs (FDR < 0.05) between the high and low *GRK6* groups in RStudio (version 3.4.4). Codes are available upon request.

2.5 Identification of top hit genes and pathway analysis

The statistically significant (FDR < 0.05) differentially expressed mRNAs in the TCGA (IlluminaHiseq) dataset that were highly expressed in the low GRK6 lung adenocarcinoma group were merged with statistically different genes in the RNA-sequencing dataset, which showed higher gene expression in si*GRK6* samples compared to the control samples by using RStudio (version 3.4.4) to identify the top hit candidate gene(s) (Fig. 2).

For pathway analysis, Metascape (https://metascape.org/gp/index.html#/main/step1) was used to detect functional enrichment of the identified top hit genes. The pathways were sorted from lowest q-value and pathways with a q-value less than 0.05 were chosen to create a histogram plot in GraphPad Prism 8.

2.6 Western blot analysis

Western blot analysis was performed with lysates from cells lysed with urea buffer (8M urea, 1M thiourea, 0.5% CHAPS, 50 mM DTT and 24 mM spermine). The bound proteins were separated on SDS polyacrylamide gels and subjected to immunoblotting with the indicated antibodies. Primary antibodies were from Proteintech (GRK6, Catalog No. 11439-1-AP, 1:1000) BD Transduction Laboratories™ (HIF1α, Catalog No. 610958, 1:1000) and Cell Signalling Technology (β-tubulin, Catalog No. 86298, 1:5000). Signals were detected using an Odyssey imaging system (LI-COR) or an ECL detection system (GE Healthcare, Chicago, IL, USA), and evaluated by ImageJ (version1.42q) software (National Institutes of Health) (Berhesda, MD, USA).

2.7 qRT-PCR

Real-time quantitative RT-PCR was performed using gene-specific primers (QuantiTect Primer Assays, Qiagen) for *CA9* (QT00011697), *NDRG1* (QT00059990) or *ACTB* (β-actin) (QT01680476) with QuantiNova SYBR Green RT-PCR kits (Qiagen). Relative transcript levels of target genes were normalised to *ACTB* (β-actin).

2.8 Clinical data and tissue samples

The study population comprised of 174 lung adenocarcinoma (LUAD) patients who were examined and treated at the Thoracic Surgery Department of the Affiliated Hospital of Nantong University and Thoracic Surgery Department of Second Affiliated Hospital of Nantong University between January 1, 2015, and December 31, 2016. The median age of patients at the time of diagnosis was 63 years (range 41–83 years). Study protocol was approved by the Ethics Committee of the Affiliated Hospital of Nantong University (No. 2018-L068), and all experiments were performed in accordance with approved guidelines of the Affiliated Hospital of Nantong University. Written informed consent was obtained from the patients for publication of this study and any accompanying images. Details of the clinical and demographic information were collected

retrospectively. All patients underwent standard surgery aiming for maximal tumour resection. Patient clinical data were recorded in detail, and the diagnoses were confirmed by at least two pathologists. Tumour histological grades and clinical stages were evaluated according to the pathological results after surgery. All tumours were staged according to the pathological tumour/node/metastasis (pTNM) classification (7th edition) of the International Union against Cancer.

2.9 Tissue microarray (TMA) construction and immunohistochemistry analysis (IHC)

Tissue microarray system (Quick-Ray, UT06, UNITMA, Korea) in the Department of Clinical Pathology, Nantong University Hospital, Jiangsu, China, was used to generate TMA. Specifically, core tissue biopsies (2 mm in diameter) were taken from individual FFPE blocks and arranged in recipient paraffin blocks. TMA specimens were cut into 4 μm sections and placed on super frost-charged glass microscope slides. TMA analysis was used as a quality control for hematoxylin and eosin staining. Tissue sections were deparaffinized and rehydrated through graded ethanol. Antigen retrieval was performed with 0.01 M citrate buffer pH 6.0 and microwave heat induction. Endogenous peroxidase activity was blocked with 3% H_2O_2 for 30 min. Sections were then incubated with a rabbit polyclonal antibody specific to GRK6 (1: 100; Proteintech, 11439-1-AP), HIF1α (1:100; Proteintech, 20960-1-AP) and VHL (1:100; Abcam, ab140989) at 4°C overnight, followed by incubation with a biotinylated anti-rabbit secondary antibody at 37 °C for 30 min. Slides were then processed using horseradish peroxidase and 3,3-diaminobenzidine chromogen solution and counterstained with hematoxylin. The staining intensity of GRK6, HIF1α or VHL for each slide was evaluated and scored by two independent pathologists. Staining intensity was scored as follows: 0 (negative), 1+ (weak staining), 2+ (moderate staining), and 3+ (intense staining). For each of the four staining intensity scores, the percentage of cells stained at each intensity were determined and intensity percentage score is the product of staining intensity and percentage of staining cells. The final staining scores were then evaluated from the sum of the four intensity percentage scores; thus, the staining score had a range from the minimum value of 0 (no staining) to a maximum of 300 (100% of cells with 3+ staining intensity), as described previously (Sun et al., 2014). The cut-off 140 was selected to evaluate: score 0–140 was considered low expression, while 141–300 was considered high expression. For all subsequent analyses, GRK6, HIF1α and VHL protein expression levels were considered either as “low” or “high” according to these cut-off values.

2.10 Statistical analysis

Two-tailed, unpaired Student’s *t-test* for the TCGA data were performed in RStudio (version 3.4.4). For multiple *t*-test, P-values were adjusted by using Benjamini-Hochberg (BH) method. Codes are available upon request. Fisher’s exact test was used to evaluate the relationship of GRK6 and HIF1α expression in lung adenocarcinoma patient samples in IHC using GraphPad Prism 8 software. $P < 0.05$ was considered statistically significant.

3 Results

3.1 Global transcriptomic changes in ATII cells upon *GRK6* depletion

We previously reported that *GRK6* knockdown promotes cell migration and invasion in lung epithelial cells (Yao et al., 2019b). To determine if, and how, lung epithelial cells responded to *GRK6* inhibition, we characterised the global transcriptomic changes in alveolar epithelial type II (ATII) cells transfected with either siRNAs against *GRK6* (si*GRK6*) or control siRNA (Control) by performing RNA sequencing (RNA-seq). Principal component analysis (PCA) showed good separation between Control compared to si*GRK6* samples (n = 3 in each group) (Supplementary Fig. 1).

Genes with a false discovery rate (FDR) adjusted *P* value (or q-value) of less than 0.05 were considered as differentially expressed genes (DEGs). In total, 7,116 DEGs were identified, including 3,430 up-regulated (Supplementary Table 1) and 3,686 down-regulated (Supplementary Table 2). We then performed gene ontology (GO) enrichment analysis of the identified DEGs using ToppGene (ToppGene Suite for gene list enrichment analysis and candidate gene prioritization) website (https://toppgene.cchmc.org/). The results were grouped into molecular function (MF), biological process (BP), and cellular component (CC). Interestingly, several disease-related pathological terms were identified, including mRNA metabolism, ribonucleoprotein complex biogenesis, and regulation of cellular response to stress (FDR < 0.05; Fig. 1A and B; Supplementary Tables 3 and 4).

3.2 Candidate pathways enriched upon *GRK6* inhibition are identified by TCGA analysis coupled with RNA-seq

To understand the role of GRK6 in lung adenocarcinoma, we performed TCGA analysis coupled with the RNA-seq data described above. As shown in Fig. 2A, correlation analysis was performed in the TCGA lung adenocarcinoma (LUAD) (IlluminaHiseq) dataset; samples were separated into high *vs.* low *GRK6* expression based on an unsupervised hierarchical clustering (Supplementary Fig. 2). We identified 2,345 genes as differentially expressed in the high *vs.* low *GRK6* samples in the TCGA dataset (Fig. 2B). A total of 7,116 genes were differentially expressed in ATII cells transfected with control siRNA or siRNA against *GRK6* (si*GRK6*) in RNA-seq, among which 3,430 up-regulated (Fig. 2C). By cross-referencing the results from the TCGA analysis with the RNA-seq analysis, we identified 274 candidate genes, which were highly expressed in low *GRK6* samples in the TCGA dataset (Fig. 3A; Supplementary Table 5) and in si*GRK6* samples in the RNA-seq analysis (Fig. 3B; Supplementary Table 6).

Metascape (https://metascape.org/gp/index.html#/main/step1) was used to investigate whether these genes were enriched in certain cellular pathways. We found that several Hallmark pathways, including mitotic spindle, epithelial mesenchymal transition (EMT), protein secretion, IL2 (interleukin 2) STAT5 (signal transducer and activator of transcription 5) signalling, glycolysis, hypoxia and TGFβ signalling, were enriched upon GRK6 inhibition in lung adenocarcinoma (Fig. 3C; Table 1).

3.3 *GRK6* inhibition induces hypoxia-inducible factor (HIF) activity in the lungs

One of the Hallmark pathways enriched upon GRK6 inhibition is 'Hallmark_Hypoxia' (FDR = 0.014; Fig. 3C; Table 1). In our RNA-seq analysis, knockdown of *GRK6* in ATII cells (Fig. 4A) led to significant increases in several hypoxia-induced genes, including *CA9* (carbonic anhydrase 9), *NDRG1* (N-Myc downstream-regulated 1), *SLC2A1* (solute carrier family 2 member 1, also known as *GLUT1*, glucose transporter 1), *P4HA1* (prolyl 4-hydroxylase subunit alpha 1) and *ENO1* (enolase 1) (Buffa et al., 2010) (Fig. 4A). A significant increase in the mRNA levels of *CA9* ($P < 0.0001$) and *NDRG1* ($P < 0.001$) were confirmed with Q-RT-PCR (Fig. 4B). In addition, the protein level of HIF1α, a key regulator of the cellular response to hypoxia (Kaelin and Ratcliffe, 2008), was significantly increased upon *GRK6* depletion in the ATII cells as shown by western blot (Fig. 4C and D; $P < 0.01$). To check how GRK6 may regulate HIF activity, the mRNA levels of HIF1α (*HIF1A*), HIF2α (*EPAS1*), HIF1β (*ARNT*) and *VHL* (Von Hippel-Lindau) were screened in the RNA-seq dataset. No changes in the expression levels of *HIF1A*, *EPAS1* and *ARNT* were observed (Fig. 4E; $P > 0.05$), while the *VHL* mRNA level was decreased upon GRK6 inhibition in ATII cells (Fig. 4E; $P < 0.001$). These findings suggest that GRK6 inhibition induces HIF activity in the lungs potentially by regulating VHL, which functions as a master regulator of HIF activity by targeting the HIFα subunit for degradation (Cockman et al., 2000; Ohh et al., 2000; Schofield and Ratcliffe, 2004; Ratcliffe, 2013).

To further validate the *in vitro* findings, the correlation between GRK6 expression and HIF1α levels or GRK6 expression and VHL levels were analysed in lung adenocarcinoma samples using tissue microarrays (Fig. 5). Representative images of low and high expression of GRK6, HIF1α or VHL in lung adenocarcinoma samples are shown in Fig. 5A, Fig. 5B and Fig. 5C, respectively. Importantly, the percentage of patients with high HIF1α expression (61%) in the low GRK6 group was significantly higher than in the high GRK6 group (41%) (Fig. 5D; $P < 0.05$), while patients with low GRK6 tended to have a low level of VHL compared to those within high GRK6 group (Fig. 5D; $P < 0.0001$).

4 Discussion

Lung cancer is the most prevalent and the leading cause of cancer death (Bray et al., 2018). Adenocarcinoma is the most common type of lung cancer, in both smokers and non-smokers, in both females and males, and represents 40% of the lung cancer cases (Denisenko et al., 2018). Lung adenocarcinoma progresses from the small airway; one of the most abundant cell types present here are alveolar type II epithelial cells, which secrete mucus and other substances (Noguchi et al., 1995). Lung adenocarcinoma is one of the most aggressive cancers and the survival rate of patients is short after diagnosis with overall survival rate less than 5 years (Denisenko et al., 2018). The major challenge for lung adenocarcinoma is its resistance to conventional radiotherapies and chemotherapies (Denisenko et al., 2018).

Hypoxia is one of the typical features of the tumour microenvironment that increases the aggressiveness of different tumours such as lung cancer (Le et al., 2006), colorectal cancer (Qureshi-Baig et al., 2020), hepatocellular carcinoma (Kung-Chun Chiu et al., 2019) and oesophageal squamous cell carcinoma (Zhang et al., 2019b). Hypoxic conditions lead to the activation of various transcription factors, such as HIF1; and the activation of downstream signalling pathways that regulate cell death, motility and proliferation (Semenza, 2012). HIF1 is a heterodimeric transcription factor, capable of controlling the cellular adaptive response to hypoxia and has two subunits; HIF1α and HIF1β (Jiang et al., 1996; Semenza, 2000). Cellular oxygen concentration regulates the protein expression of HIF1α so is a key factor for cellular adaptive response to hypoxia (Jiang et al., 1996). HIF activities can also be up-regulated by other mechanisms (Zhao et al., 2014; Zhang et al., 2019c).

G protein-coupled receptor kinases (GRKs) are a family of kinases which can desensitize G protein-coupled receptors (GPCRs) homologous (Vroon et al., 2006). GRK6 is of the members of the GRK family (Willets et al., 2002; Ahmed et al., 2010; Tiedemann et al., 2010) and we previously showed that GRK6 is down-regulated in lung adenocarcinoma, which is associated with malignant tumour progression (Yao et al., 2016, 2019b), by an unknown mechanism.

To identify global transcriptomic changes in ATII cells upon *GRK6* depletion, RNA-seq coupled with siRNA-mediated depletion of *GRK6* was performed in ATII cells. We identified 3,430 up-regulated and 3,686 down-regulated DEGs. GO functional analysis with DEGs demonstrated that DEGs are mainly enriched in mRNA metabolism, ribonucleoprotein complex biogenesis, and regulation of cellular response to stress. To understand the role of GRK6 in lung adenocarcinoma, analysis of TCGA data was coupled with the RNA-seq data, described above. Pathway analysis suggested that one of the Hallmark pathways enriched upon GRK6 inhibition is 'Hallmark_Hypoxia'. We demonstrated that *GRK6* depletion induces HIF1α expression and activity in ATII cells. The findings were further confirmed in lung adenocarcinoma samples, in which GRK6 expressions negatively correlate with HIF1α protein levels. Mechanistically, the impact of GRK6 on HIF activity could be achieved via regulation of VHL levels, which is a master regulator of HIF activity by targeting the prolyl-hydroxylated HIF1α subunit for ubiquitylation and rapid proteasomal degradation (Cockman et al., 2000; Ohh et al., 2000; Schofield and Ratcliffe, 2004; Ratcliffe, 2013). This study provides evidence that GRK6 inhibition causes a decrease in VHL expression, leading to HIFα stabilisation with increased activity in lung adenocarcinoma, although the underlying mechanism merits further investigation.

Earlier reports suggest that hypoxia regulates mRNA translation (Liu et al., 2006). RNA-binding proteins (heterogeneous nuclear ribonucleoproteins) have a role in post-transcriptional gene

regulation under hypoxic conditions and are associated with hypoxia-induced transcripts that regulate encoded protein levels (Yang et al., 2006). Hypoxia can affect tumour cells; by acting as a stressor and inhibiting cell growth or inducing cell death. Alternatively, it can act by contributing to carcinogenesis progression and resistance to treatments, leading to hypoxia-induced genomic and proteomic changes in the cancer cells (Höckel and Vaupel, 2001; Vaupel et al., 2001).

We previously demonstrated that cell migration and invasion in lung epithelial cells is induced upon *GRK6* knockdown (Yao et al., 2019b). In addition to the hypoxia, this analysis showed EMT is also enriched upon *GRK6* inhibition, which can explain our previous findings (Yao et al., 2019b). The hypoxic tumour microenvironment can regulate EMT (Wei et al., 2016; Joseph et al., 2018). EMT is a biological process and the cell polarity and cell-cell adhesion of epithelial cells are lost and in turn become mesenchymal cells, which have migratory and invasive features (Polyak and Weinberg, 2009). In a similar manner to our findings (Yao et al., 2019b), previous studies in medulloblastoma (Yuan et al., 2013) and Lewis lung carcinoma (Raghuwanshi et al., 2013) show that when *GRK6* was downregulated, migration and metastasis were increased. Consistently, it has been found that hypoxia-related genes *CA9*, *NDRG1*, *SLC2A1*, *P4HA1* and *ENO1* induced EMT in hepatocellular carcinoma (Hyuga et al., 2017), bladder cancer (Li et al., 2019), laryngeal cancer (Starska et al., 2015) and gastric cancer (Xu et al., 2019; Zhang et al., 2019a), respectively. Our study showed an increase of hypoxia-induced gene expression and HIF1α expression in *GRK6* knockdown cells, this suggests that *GRK6* knockdown may induce EMT in lung adenocarcinoma.

In summary, this study shows that *GRK6* is involved in different disease-related pathological features; mRNA metabolism, ribonucleoprotein complex biogenesis, regulation of cellular response to stress, as well as EMT and hypoxia. Targeting the HIF pathway may provide new strategies for therapy in *GRK6*-depleted lung adenocarcinoma patients.

5 Data availability Statement

RNA-seq data associated with this study have been deposited in the Gene Expression Omnibus (GEO) database (accession code GSE164921).

6 Ethics Statement

This study was approved by the Ethics Committee of the Affiliated Hospital of Nantong University (No. 2018-L068).

7 Author Contributions

Conceptualization: Y.W, Y.L, X.L; Investigation: S.Y, A.E, Y.Z, L.Y, C.H, J.C, Y.G, H.S; Formal analysis: S.Y, A.E, Y.Z, H.S, Y.W; Writing: A.E, S.Y, Y.Z, L.Y, C.H with support from Y.W and R.M.E; Supervision: Y.W, Y.L, X.L; Funding acquisition: Y.W, Y.L, S.Y.

8 Funding

This project was funded by grants from Medical Research Council (UK) [MR/S025480/1], Jiangsu Post-doctoral Foundation Research Project, China [No. 2019Z142], Key Talents of Medical Science in Jiangsu Province, China [No. QNRC2016682], and Science and Technology Project of Nantong [No. JCZ18130]. AE was supported by the Wessex Medical Trust. YZ was supported by an Institute for Life Sciences (University of Southampton) PhD Studentship. CH was supported by Gerald Kerkut Charitable Trust and University of Southampton Central VC Scholarship Scheme. We thank Prof. Julian Downward (The Francis Crick Institute, UK) for providing ATII cells.

9 References

Ahmed, M. R., Berthet, A., Bychkov, E., Porras, G., Li, Q., Bioulac, B. H., et al. (2010). Lentiviral overexpression of GRK6 alleviates L-dopa-induced dyskinesia in experimental Parkinson's disease. *Science Translational Medicine* 2(28), 28ra28. doi:10.1126/scitranslmed.3000664.

Balabanian, K., Lagane, B., Pablos, J. L., Laurent, L., Planchenault, T., Verola, O., et al. (2005). WHIM syndromes with different genetic anomalies are accounted for by impaired CXCR4 desensitization to CXCL12. *Blood* 105(6), 2449–2457. doi:10.1182/blood-2004-06-2289.

Barak, L. S., Oakley, R. H., Laporte, S. A., and Caron, M. G. (2001). Constitutive arrestin-mediated desensitization of a human vasopressin receptor mutant associated with nephrogenic diabetes insipidus. *Proceedings of the National Academy of Sciences of the United States of America* 98(1), 93–98. doi:10.1073/pnas.98.1.93.

Bouvier, M., Hausdorff, W. P., De Blasi, A., O'Dowd, B. F., Kobilka, B. K., Caron, M. G., et al. (1988). Removal of phosphorylation sites from the β2-adrenergic receptor delays onset of agonist-promoted desensitization. *Nature* 333(6170), 370–373. doi:10.1038/333370a0.

Bray, F., Ferlay, J., Soerjomataram, I., Siegel, R. L., Torre, L. A., and Jemal, A. (2018). Global cancer statistics 2018: GLOBOCAN estimates of incidence and mortality worldwide for 36 cancers in 185 countries. *CA: a cancer journal for clinicians* 68(6), 394–424. doi:10.3322/caac.21492.

Buffa, F. M., Harris, A. L., West, C. M., and Miller, C. J. (2010). Large meta-analysis of multiple cancers reveals a common, compact and highly prognostic hypoxia metagene. *British Journal of Cancer* 102(2), 428–435. doi:10.1038/sj.bjc.6605450.

Cockman, M. E., Masson, N., Mole, D. R., Jaakkola, P., Chang, G. W., Clifford, S. C., et al. (2000). Hypoxia inducible factor-α binding and ubiquitylation by the von Hippel-Lindau tumor suppressor protein. *Journal of Biological Chemistry* 275(33), 25733–25741. doi:10.1074/jbc.M002740200.

Coelho, M. A., de Carné Trécesson, S., Rana, S., Zecchin, D., Moore, C., Molina-Arcas, M., et al. (2017). Oncogenic RAS Signaling Promotes Tumor Immunoresistance by Stabilizing PD-L1 mRNA. *Immunity* 47(6), 1083-1099.e6. doi:10.1016/j.immuni.2017.11.016.

Denisenko, T. V., Budkevich, I. N., and Zhivotovsky, B. (2018). Cell death-based treatment of lung adenocarcinoma. *Cell Death and Disease* 9(2), 117. doi:10.1038/s41419-017-0063-y.

Ewels, P., Magnusson, M., Lundin, S., and Käller, M. (2016). MultiQC: Summarize analysis results for multiple tools and samples in a single report. *Bioinformatics* 32(19), 3047–3048. doi:10.1093/bioinformatics/btw354.

Gainetdinov, R. R., Bohn, L. M., Sotnikova, T. D., Cyr, M., Laakso, A., Macrae, A. D., et al. (2003). Dopaminergic supersensitivity in G protein-coupled receptor kinase 6-deficient mice. *Neuron* 38(2), 291–303. doi:10.1016/S0896-6273(03)00192-2.

Hill, C., Li, J., Liu, D., Conforti, F., Brereton, C. J., Yao, L., et al. (2019). Autophagy inhibition-mediated epithelial–mesenchymal transition augments local myofibroblast differentiation in pulmonary fibrosis. *Cell Death and Disease* 10(8), 591. doi:10.1038/s41419-019-1820-x.

Höckel, M., and Vaupel, P. (2001). Tumor hypoxia: Definitions and current clinical, biologic, and molecular aspects. *Journal of the National Cancer Institute* 93(4), 266–276. doi:10.1093/jnci/93.4.266.

Hyuga, S., Wada, H., Eguchi, H., Otsuru, T., Iwgami, Y., Yamada, D., et al. (2017). Expression of carbonic anhydrase IX is associated with poor prognosis through regulation of the epithelial-mesenchymal transition in hepatocellular carcinoma. *International Journal of Oncology* 51(4), 1179–1190. doi:10.3892/ijo.2017.4098.

Jiang, B. H., Semenza, G. L., Bauer, C., and Marti, H. H. (1996). Hypoxia-inducible factor 1 levels vary exponentially over a physiologically relevant range of O2 tension. *American Journal of Physiology - Cell Physiology* 271(4), C1172-1180. doi:10.1152/ajpcell.1996.271.4.c1172.

Joseph, J. P., Harishankar, M. K., Pillai, A. A., and Devi, A. (2018). Hypoxia induced EMT: A review on the mechanism of tumor progression and metastasis in OSCC. *Oral Oncology* 80(1), 23–32. doi:10.1016/j.oraloncology.2018.03.004.

Kaelin, W. G., and Ratcliffe, P. J. (2008). Oxygen sensing by metazoans: the central role of the HIF hydroxylase pathway. *Molecular Cell* 30(4), 393–402. doi:10.1016/j.molcel.2008.04.009.

Kim, D., Langmead, B., and Salzberg, S. L. (2015). HISAT: A fast spliced aligner with low memory requirements. *Nature Methods* 12(4), 357–360. doi:10.1038/nmeth.3317.

Kung-Chun Chiu, D., Pui-Wah Tse, A., Law, C. T., Ming-Jing Xu, I., Lee, D., Chen, M., et al. (2019). Hypoxia regulates the mitochondrial activity of hepatocellular carcinoma cells through HIF/HEY1/PINK1 pathway. *Cell Death and Disease* 10(12), 934. doi:10.1038/s41419-019-2155-3.

Le, Q. T., Chen, E., Salim, A., Cao, H., Kong, C. S., Whyte, R., et al. (2006). An evaluation of tumor oxygenation and gene expression in patients with early stage non-small cell lung cancers. *Clinical Cancer Research* 12(5), 1507–1514. doi:10.1158/1078-0432.CCR-05-2049.

Li, A., Zhu, X., Wang, C., Yang, S., Qiao, Y., Qiao, R., et al. (2019). Upregulation of NDRG1 predicts poor outcome and facilitates disease progression by influencing the EMT process in bladder cancer. *Scientific Reports* 9(1), 5166. doi:10.1038/s41598-019-41660-w.

Li, H., Handsaker, B., Wysoker, A., Fennell, T., Ruan, J., Homer, N., et al. (2009). The Sequence Alignment/Map format and SAMtools. *Bioinformatics* 25(16), 2078–2079. doi:10.1093/bioinformatics/btp352.

Li, Y. P. (2013). GRK6 expression in patients with hepatocellular carcinoma. *Asian Pacific Journal of Tropical Medicine* 6(3), 220–223. doi:10.1016/S1995-7645(13)60027-9.

Liao, Y., Smyth, G. K., and Shi, W. (2014). FeatureCounts: An efficient general purpose program for assigning sequence reads to genomic features. *Bioinformatics* 30(7), 923–930. doi:10.1093/bioinformatics/btt656.

421 Liu, L., Cash, T. P., Jones, R. G., Keith, B., Thompson, C. B., and Simon, M. C. (2006). Hypoxia-
422 induced energy stress regulates mRNA translation and cell growth. *Molecular Cell* 21(4), 521–
423 531. doi:10.1016/j.molcel.2006.01.010.

424 Love, M. I., Huber, W., and Anders, S. (2014). Moderated estimation of fold change and dispersion
425 for RNA-seq data with DESeq2. *Genome Biology* 15(12), 550. doi:10.1186/s13059-014-0550-8.

426 Molina-Arcas, M., Hancock, D. C., Sheridan, C., Kumar, M. S., and Downward, J. (2013).
427 Coordinate direct input of both KRAS and IGF1 receptor to activation of PI3 kinase in KRAS -
428 mutant lung cancer. *Cancer Discovery* 3(5), 548–563. doi:10.1158/2159-8290.CD-12-0446.

429 Noguchi, M., Morikawa, A., Kawasaki, M., Matsuno, Y., Yamada, T., Hirohashi, S., et al. (1995).
430 Small adenocarcinoma of the lung. Histologic characteristics and prognosis. *Cancer* 75(12),
431 2844–2852. doi:10.1002/1097-0142(19950615)75:12<2844::aid-cncr2820751209>3.0.co;2-#.

432 Ohh, M., Park, C. W., Ivan, M., Hoffman, M. A., Kim, T. Y., Huang, L. E., et al. (2000).
433 Ubiquitination of hypoxia-inducible factor requires direct binding to the β-domain of the von
434 Hippel - Lindau protein. *Nature Cell Biology* 2(7), 423–427. doi:10.1038/35017054.

435 Polyak, K., and Weinberg, R. A. (2009). Transitions between epithelial and mesenchymal states:
436 acquisition of malignant and stem cell traits. *Nature Reviews Cancer* 9(4), 265–273.
437 doi:10.1038/nrc2620.

438 Qiu, X., Chen, J., Zhang, Z., You, Y., and Wang, Z. (2016). Aberrant GRK6 promoter methylation is
439 associated with poor prognosis in hypopharyngeal squamous cell carcinoma. *Oncology Reports*
440 35(2), 1027–1033. doi:10.3892/or.2015.4469.

441 Qureshi-Baig, K., Kuhn, D., Viry, E., Pozdeev, V. I., Schmitz, M., Rodriguez, F., et al. (2020).
442 Hypoxia-induced autophagy drives colorectal cancer initiation and progression by activating the
443 PRKC/PKC-EZR (ezrin) pathway. *Autophagy* 16(8), 1436–1452.
444 doi:10.1080/15548627.2019.1687213.

445 Raghuwanshi, S. K., Smith, N., Rivers, E. J., Thomas, A. J., Sutton, N., Hu, Y., et al. (2013). GRK6
446 deficiency promotes angiogenesis, tumor progression and metastasis. *Journal of immunology*
447 190(10), 5329–5336. doi:10.4049/jimmunol.1202058.GRK6.

448 Ratcliffe, P. J. (2013). Oxygen sensing and hypoxia signalling pathways in animals : the implications
449 of physiology for cancer. *The Journal of physiology* 591(8), 2027–2042.
450 doi:10.1113/jphysiol.2013.251470.

451 Rockman, H. A., Chien, K. R., Choi, D. J. U., Iaccarino, G., Hunter, J. J., John Ross, J. R., et al.
452 (1998). Expression of a β-adrenergic receptor kinase 1 inhibitor prevents the development of
453 myocardial failure in gene-targeted mice. *Proceedings of the National Academy of Sciences of*
454 *the United States of America* 95(12), 7000–7005. doi:10.1073/pnas.95.12.7000.

455 Schofield, C. J., and Ratcliffe, P. J. (2004). Oxygen sensing by HIF hydroxylases. *Nature Reviews*
456 *Molecular Cell Biology* 5(5), 343–354. doi:10.1038/nrm1366.

457 Semenza, G. L. (2000). Hypoxia, clonal selection, and the role of HIF-1 in tumor progression.
458 *Critical Reviews in Biochemistry and Molecular Biology* 35(2), 71–103.

doi:10.1080/10409230091169186.

Semenza, G. L. (2012). Hypoxia-inducible factors: mediators of cancer progression and targets for cancer therapy. *Trends in Pharmacological Sciences* 33(4), 207–214. doi:10.1016/j.tips.2012.01.005.

Starska, K., Forma, E., Jóźwiak, P., Bryś, M., Lewy-Trenda, I., Brzezińska-Błaszczyk, E., et al. (2015). Gene and protein expression of glucose transporter 1 and glucose transporter 3 in human laryngeal cancer—the relationship with regulatory hypoxia-inducible factor-1α expression, tumor invasiveness, and patient prognosis. *Tumor Biology* 36(4), 2309–2321. doi:10.1007/s13277-014-2838-4.

Sun, R., Wang, X., Zhu, H., Mei, H., Wang, W., Zhang, S., et al. (2014). Prognostic value of LAMP3 and TP53 overexpression in benign and malignant gastrointestinal tissues. *Oncotarget* 5(23), 12398–12409. doi:10.18632/oncotarget.2643.

Tao, R., Li, Q., Gao, X., and Ma, L. (2018). Overexpression of GRK6 associates with the progression and prognosis of colorectal carcinoma. *Oncology Letters* 15(4), 5879–5886. doi:10.3892/ol.2018.8030.

Tiedemann, R. E., Zhu, Y. X., Schmidt, J., Yin, H., Shi, C. X., Que, Q., et al. (2010). Kinome-wide RNAi studies in human multiple myeloma identify vulnerable kinase targets, including a lymphoid-restricted kinase, GRK6. *Blood* 115(8), 1594–1604. doi:10.1182/blood-2009-09-243980.

Vaupel, P., Thews, O., and Hoeckel, M. (2001). Treatment resistance of solid tumors: Role of hypoxia and anemia. *Medical Oncology* 18(4), 243–259. doi:10.1385/MO:18:4:243.

Vroon, A., Heijnen, C. J., and Kavelaars, A. (2006). GRKs and arrestins: regulators of migration and inflammation. *Journal of Leukocyte Biology* 80(6), 1214–1221. doi:10.1189/jlb.0606373.

Wang, W. C. H., Mihlbachler, K. A., Brunnett, A. C., and Liggett, S. B. (2009). Targeted transgenesis reveals discrete attenuator functions of GRK and PKA in airway β2-adrenergic receptor physiologic signaling. *Proceedings of the National Academy of Sciences of the United States of America* 106(35), 15007–15012. doi:10.1073/pnas.0906034106.

Wei, L., Sun, J. J., Cui, Y. C., Jiang, S. L., Wang, X. W., Lv, L. Y., et al. (2016). Twist may be associated with invasion and metastasis of hypoxic NSCLC cells. *Tumor Biology* 37(7), 9979–9987. doi:10.1007/s13277-016-4896-2.

Willets, J. M., John Challiss, R. A., and Nahorski, S. R. (2002). Endogenous G protein-coupled receptor kinase 6 regulates M3 muscarinic acetylcholine receptor phosphorylation and desensitization in human SH-SY5Y neuroblastoma cells. *Journal of Biological Chemistry* 277(18), 15523–15529. doi:10.1074/jbc.M111217200.

Xu, X., Chen, B., Zhu, S., Zhang, J., He, X., Cao, G., et al. (2019). Hyperglycemia promotes Snail-induced epithelial-mesenchymal transition of gastric cancer via activating ENO1 expression. *Cancer Cell International* 19(1), 344. doi:10.1186/s12935-019-1075-8.

Yang, R., Weber, D. J., and Carrier, F. (2006). Post-transcriptional regulation of thioredoxin by the

stress inducible heterogenous ribonucleoprotein A18. *Nucleic Acids Research* 34(4), 1224–1236. doi:10.1093/nar/gkj519.

Yao, L., Conforti, F., Hill, C., Bell, J., Drawater, L., Li, J., et al. (2019a). Paracrine signalling during ZEB1-mediated epithelial–mesenchymal transition augments local myofibroblast differentiation in lung fibrosis. *Cell Death and Differentiation* 26(5), 943–957. doi:10.1038/s41418-018-0175-7.

Yao, S., Wu, D., Chen, J., Wang, P., Lv, X., and Huang, J. (2019b). Hypermethylation of the G protein-coupled receptor kinase 6 (GRK6) promoter inhibits binding of C/EBPα, and GRK6 knockdown promotes cell migration and invasion in lung adenocarcinoma cells. *FEBS Open Bio* 9(4), 605–617. doi:10.1002/2211-5463.12606.

Yao, S., Zhong, L., Liu, J., Feng, J., Bian, T., Zhang, Q., et al. (2016). Prognostic value of decreased GRK6 expression in lung adenocarcinoma. *Journal of Cancer Research and Clinical Oncology* 142(12), 2541–2549. doi:10.1007/s00432-016-2244-y.

Yu, S., Sun, L., Jiao, Y., and Lee, L. T. O. (2018). The role of G protein-coupled receptor kinases in cancer. *International Journal of Biological Sciences* 14(2), 189–203. doi:10.7150/ijbs.22896.

Yuan, L., Zhang, H., Liu, J., Rubin, J. B., Cho, Y. J., Shu, H. K., et al. (2013). Growth factor receptor-Src-mediated suppression of GRK6 dysregulates CXCR4 signaling and promotes medulloblastoma migration. *Molecular Cancer* 12(1), 18. doi:10.1186/1476-4598-12-18.

Zhang, J., Guo, S., Wu, Y., Zheng, Z. C., Wang, Y., and Zhao, Y. (2019a). P4HB, a Novel Hypoxia Target Gene Related to Gastric Cancer Invasion and Metastasis. *BioMed Research International* 2019(1), 9749751. doi:10.1155/2019/9749751.

Zhang, Q., Zhang, J., Fu, Z., Dong, L., Tang, Y., Xu, C., et al. (2019b). Hypoxia-induced microRNA-10b-3p promotes esophageal squamous cell carcinoma growth and metastasis by targeting TSGA10. *Aging* 11(22), 10374–10384. doi:10.18632/aging.102462.

Zhang, W. C., Wells, J. M., Chow, K.-H., Huang, H., Yuan, M., Saxena, T., et al. (2019c). miR-147b-mediated TCA cycle dysfunction and pseudohypoxia initiate drug tolerance to EGFR inhibitors in lung adenocarcinoma. *Nature Metabolism* 1(4), 460–474. doi:10.1038/s42255-019-0052-9.

Zhao, F., Malm, S. W., Hinchman, A. N., Li, H., Beeks, C. G., and Klimecki, W. T. (2014). Arsenite-induced pseudo-hypoxia results in loss of anchorage-dependent growth in BEAS-2B pulmonary epithelial cells. *PLoS ONE* 9(12), e114549. doi:10.1371/journal.pone.0114549.

10 Figure Legends

10.1 FIGURE 1 | Global transcriptomic changes in ATII cells upon *GRK6* depletion. (A) REVIGO TreeMap showing Gene Ontology (GO) analysis of upregulated differentially expressed genes (DEGs) in ATII cells transfected with siRNAs against *GRK6 vs.* control siRNA. Common colours represent groupings based on parent GO terms, and each rectangle is proportional to the relative enrichment of the GO term compared to the whole genome. Genes with false discovery rate (FDR) < 0.05 were considered as DEGs (differentially expressed genes). (B) Scatter plot showing the top 10 enriched GO terms from 3 categories (biological process, cellular component and molecular function) according to rich factors. Rich factor is the percentage of DEGs enriched gene count in the given annotated GO terms. The sizes of circles represent gene counts, and the colours of circles represent the $-\text{Log}_{10}$ of the adjusted *P*-values (padj). Values less than 0.05 were considered as statistically significant.

10.2 FIGURE 2 | The analysis to identify candidate genes upon *GRK6* inhibition. (A) In brief, TCGA analysis coupled to RNA sequencing in ATII cells upon *GRK6* depletion (si*GRK6*) was used (details in Methods). FDR: false discovery rate. (B) Heat-map showing DEGs (differentially expressed genes) between low GRK6 (n = 26) and high GRK6 (n = 17) expressing lung adenocarcinoma samples from TCGA analysis. Red indicates up-regulation and blue down-regulation. Genes with false discovery rate (FDR) adjusted P-values less than 0.05 were considered as DEGs. P-values were adjusted by using Benjamini-Hochberg (BH) method. (C) Heat-map showing DEGs in ATII cells transfected with siRNA against GRK6 (si*GRK6*) *vs.* control siRNA (Control). Red indicates up-regulation and blue down-regulation. n = 3 samples per group. DESeq2 Wald test was performed for statistical analysis. Genes with false discovery rate (FDR) adjusted P-values less than 0.05 were considered as DEGs. P-values were adjusted by using Benjamini-Hochberg (BH) method.

10.3 FIGURE 3 | Candidate pathways enriched upon *GRK6* inhibition are identified by TCGA analysis coupled to RNA sequencing. (A) Heat-map showing genes that are over-expressed in lung adenocarcinoma samples with low GRK6 (n = 26) compared to those with high GRK6 (n = 17) from TCGA analysis. Red indicates up-regulation and blue down-regulation. Genes with false discovery rate (FDR) adjusted P-values less than 0.05 were considered as DEGs. P-values were adjusted by using Benjamini-Hochberg (BH) method. (B) Heat-map showing DEGs (differentially expressed genes) that are over-expressed in ATII cells transfected with siRNA against *GRK6* (si*GRK6*) *vs.* control siRNA. Red indicates up-regulation and blue down-regulation. n = 3 samples per group. DESeq2 Wald test was performed for statistical analysis. Genes with false discovery rate (FDR) adjusted P-values less than 0.05 were considered as DEGs. P-values were adjusted by using Benjamini-Hochberg (BH) method. (C) Pathways enriched upon *GRK6* inhibition were visualised on a bar chart, showing number of shared genes and $-\text{Log}_{10}$ (q value).

10.4 FIGURE 4 | *GRK6* depletion induces HIF (hypoxia-inducible factors) activity in ATII (alveolar epithelial type II) cells. (A) RNA-seq showing relative expressions of *GRK6*, *CA9, NDRG1, SLC2A1, P4HA1* and *ENO1* in ATII cells transfected with control or *GRK6* siRNA. Data are mean ± s.d. n = 3 samples per group. Multiple t-test was performed for statistical analysis. Genes with false discovery rate (FDR) adjusted P-values less than 0.05 were considered as DEGs. P-values were adjusted by using Benjamini-Hochberg (BH) method. B)

Fold change in mRNA levels of *CA9* and *NDRG1* in ATII cells transfected with control or *GRK6* siRNA. *ACTB* (β-actin)-normalised mRNA levels in control cells were used to set the baseline value at unity. Data are mean ± s.d. $n = 3$ samples per group. Multiple t-test was performed for statistical analysis. Genes with false discovery rate (FDR) adjusted P-values less than 0.05 were considered as DEGs. P-values were adjusted by using Benjamini-Hochberg (BH) method. (C) Protein expression of HIF1α and GRK6 in ATII cells transfected with control or *GRK6* siRNA. β-tubulin was used as a loading control. (D) Quantification of Figure 4C. Graph showing protein level of HIF1α in ATII cell line with indicated transfections. Data are mean ± s.d. $n = 3$ per group. Two tailed, unpaired Student's *t-test* was performed for statistical analysis. P-value less than 0.05 was considered as statistically significant. (E) RNA-seq showing relative expressions of *HIF1A*, *ARNT, EPAS1* and *VHL* in ATII cells transfected with control or *GRK6* siRNA. Data are mean ± s.d. $n = 3$ samples per group. Multiple t-test was performed for statistical analysis. Genes with false discovery rate (FDR) adjusted P-values less than 0.05 were considered as DEGs. P-values were adjusted by using Benjamini-Hochberg (BH) method.

10.5 FIGURE 5 | GRK6 expression levels negatively and positively correlate with HIF1α and VHL expressions in lung adenocarcinoma, respectively. (A) Representative GRK6 staining pattern (low or high GRK6) in lung adenocarcinoma tissue microarray cores. Scale bar: 500 µm. (B) Representative HIF1α staining pattern (low or high HIF1α) in lung adenocarcinoma tissue microarray cores. Scale bar: 500 µm. (C) Representative VHL staining pattern (low or high VHL) in lung adenocarcinoma tissue microarray cores. Scale bar: 500 µm. (D) Graph showing the number and percentage of lung adenocarcinoma patients with low/high HIF1α or low/high VHL in high *vs.* low GRK6 group. High GRK6 n =82. Low GRK6 $n = 92$. Fisher's exact test was performed for statistical analysis. P-values less than 0.05 were considered as statistically significant.

11 Tables

11.1 Table 1

Table 1 | List of pathways enriched upon GRK6 inhibition.

	Number of shared genes	-Log_{10} (q-value)	Genes
HALLMARK MITOTIC SPINDLE	13	4.653	*APC, ARHGAP5, NOTCH2, RFC1, ROCK1, TIAM1, TRIO, ARHGAP29, RASAL2, ARHGEF12, SUN2, DYNLL2, PPP4R2*
HALLMARK EPITHELIAL MESENCHYMAL TRANSITION	12	4.122	*CALU, CD44, CD59, DPYSL3, FBN2, FN1, ITGAV, NOTCH2, PTX3, SDC1, TGFBI, SLIT2*
HALLMARK PROTEIN SECRETION	8	3.664	*CLCN3, GOLGA4, IGF2R, PAM, RPS6KA3, ZW10, SCRN1, STX12*
HALLMARK UV RESPONSE DN	9	3.321	*RUNX1, LTBP1, NOTCH2, ATXN1, NRP1, MAGI2, NR1D2, SIPA1L1, MIOS*
HALLMARK IL2 STAT5 SIGNALING	10	3.042	*CD44, IGF2R, ITGAV, PRNP, TIAM1, NRP1, DENND5A, TWSG1, RRAGD, SPRED2*
HALLMARK GLYCOLYSIS	9	2.418	*CD44, ENO1, IL13RA1, PAM, SDC1, TGFBI, P4HA2, HS2ST1, RRAGD*
HALLMARK HYPOXIA	8	1.847	*ENO1, GBE1, PAM, PFKFB3, TGFBI, P4HA2, KDM3A, RRAGD*
HALLMARK TGF BETA SIGNALING	4	1.701	*ACVR1, APC, SLC20A1, NOG*

12 Table Legends

12.1 Table 1 List of pathways enriched upon GRK6 inhibition.

Figure 1

A

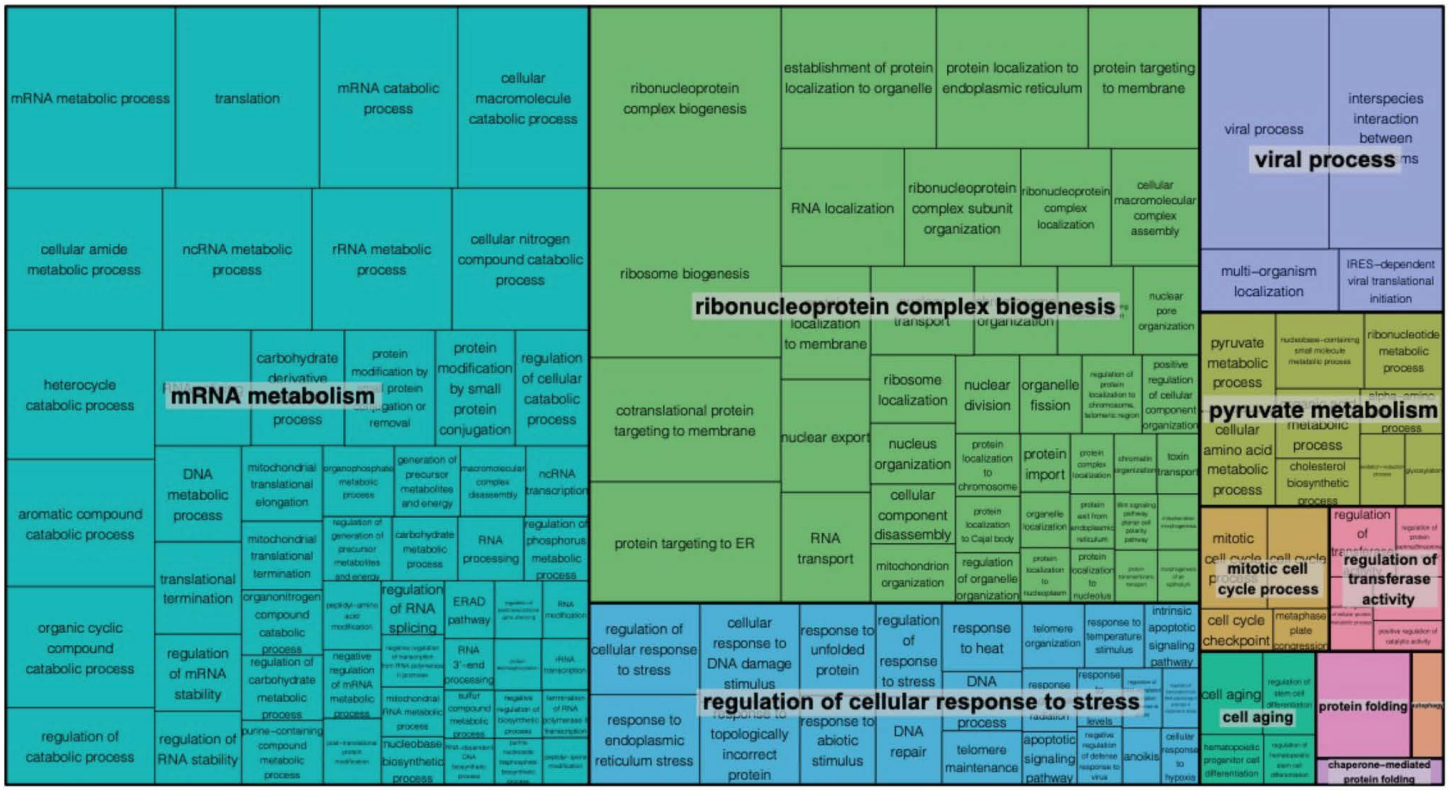
mRNA metabolic process
translation
mRNA catabolic process
cellular macromolecule catabolic process
cellular amide metabolic process
ncRNA metabolic process
rRNA metabolic process
cellular nitrogen compound catabolic process
heterocycle catabolic process
mRNA metabolism
carbohydrate derivative process
protein modification by small protein conjugation or removal
protein modification by small protein conjugation
regulation of cellular catabolic process
aromatic compound catabolic process
DNA metabolic process
translational termination
organic cyclic compound catabolic process
regulation of mRNA stability
regulation of catabolic process
regulation of RNA stability
mitochondrial translational elongation
mitochondrial translational termination
organonitrogen compound catabolic process
regulation of carbohydrate metabolic process
purine-containing compound metabolic process
carbohydrate metabolic process
RNA processing
regulation of phosphorus metabolic process
regulation of RNA splicing
ERAD pathway
RNA 3'-end processing
nucleobase biosynthetic process
ncRNA transcription
ribonucleoprotein complex biogenesis
establishment of protein localization to organelle
protein localization to endoplasmic reticulum
protein targeting to membrane
RNA localization
ribonucleoprotein complex subunit organization
ribonucleoprotein complex localization
cellular macromolecular complex assembly
ribosome biogenesis
ribonucleoprotein complex biogenesis
nuclear pore organization
cotranslational protein targeting to membrane
nuclear export
protein targeting to ER
RNA transport
ribosome localization
nuclear division
organelle fission
nucleus organization
protein import
cellular component disassembly
mitochondrion organization
regulation of cellular response to stress
cellular response to DNA damage stimulus
response to unfolded protein
regulation of response to stress
response to heat
telomere organization
response to temperature stimulus
intrinsic apoptotic signaling pathway
response to endoplasmic reticulum stress
response to topologically incorrect protein
response to abiotic stimulus
DNA repair
telomere maintenance
apoptotic signaling pathway
anoikis
viral process
interspecies interaction between
multi-organism localization
IRES-dependent viral translational initiation
pyruvate metabolic process
ribonucleotide metabolic process
pyruvate metabolism
cellular amino acid metabolic process
cholesterol biosynthetic process
mitotic cell cycle process
regulation of transferase activity
cell cycle checkpoint
cell aging
protein folding
chaperone-mediated protein folding

B

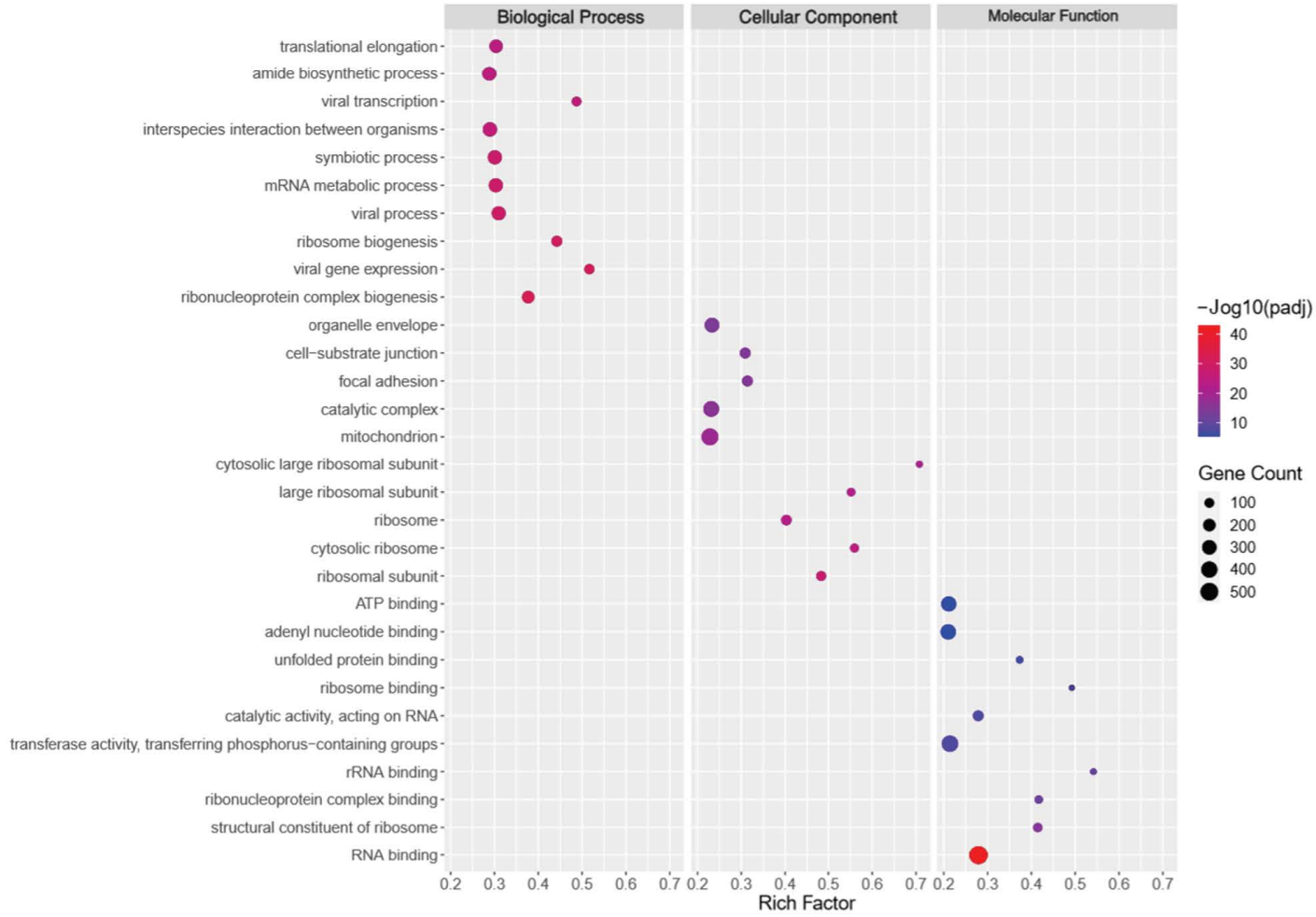
Biological Process
Cellular Component
Molecular Function
translational elongation
amide biosynthetic process
viral transcription
interspecies interaction between organisms
symbiotic process
mRNA metabolic process
viral process
ribosome biogenesis
viral gene expression
ribonucleoprotein complex biogenesis
organelle envelope
cell-substrate junction
focal adhesion
catalytic complex
mitochondrion
cytosolic large ribosomal subunit
large ribosomal subunit
ribosome
cytosolic ribosome
ribosomal subunit
ATP binding
adenyl nucleotide binding
unfolded protein binding
ribosome binding
catalytic activity, acting on RNA
transferase activity, transferring phosphorus-containing groups
rRNA binding
ribonucleoprotein complex binding
structural constituent of ribosome
RNA binding
0.2
0.3
0.4
0.5
0.6
0.7
Rich Factor
−Jog10(padj)
40
30
20
10
Gene Count
100
200
300
400
500

Figure 2

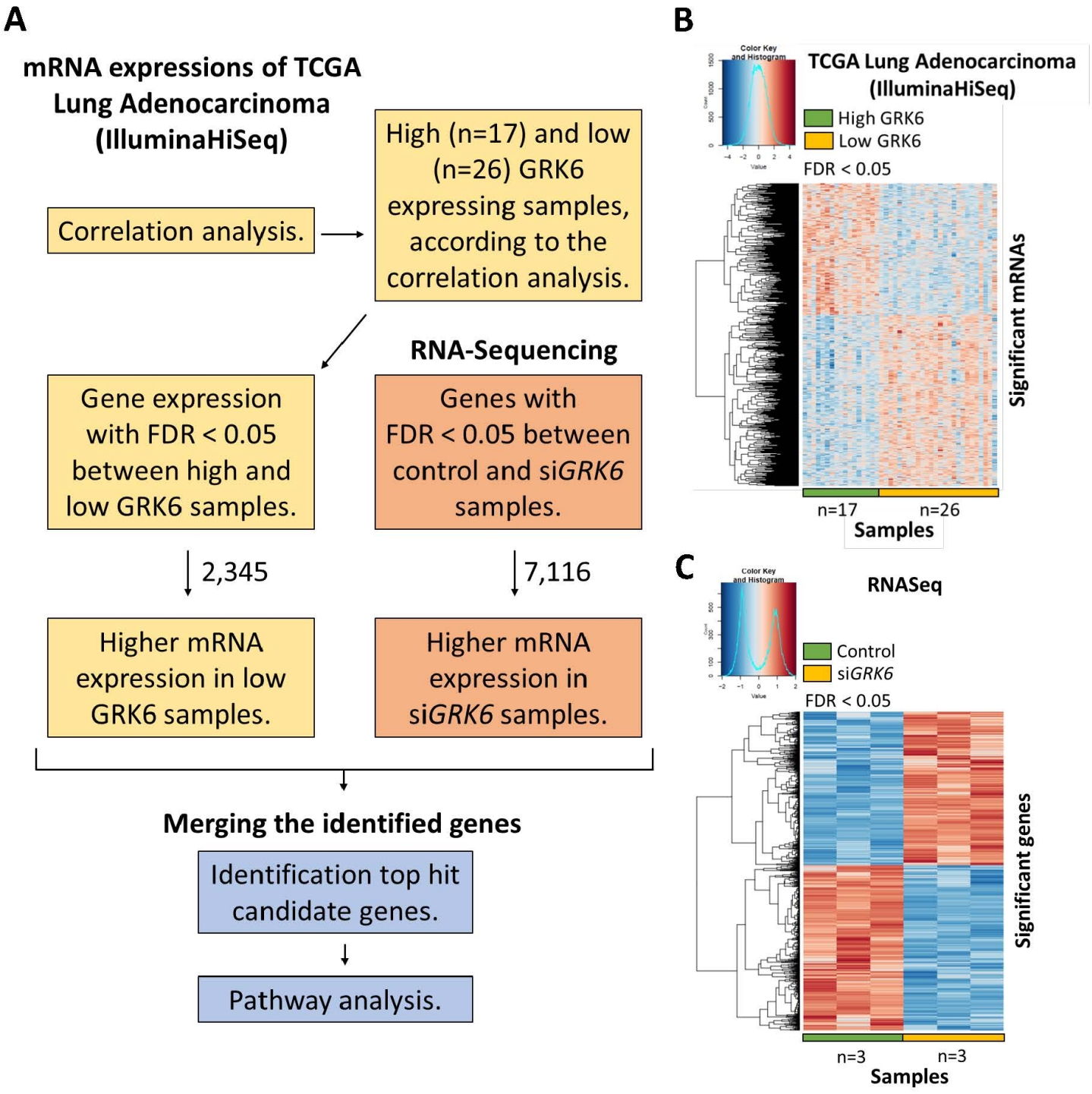
A
mRNA expressions of TCGA Lung Adenocarcinoma (IlluminaHiSeq)
Correlation analysis.
High (n=17) and low (n=26) GRK6 expressing samples, according to the correlation analysis.
RNA-Sequencing
Gene expression with FDR < 0.05 between high and low GRK6 samples.
Genes with FDR < 0.05 between control and siGRK6 samples.
2,345
7,116
Higher mRNA expression in low GRK6 samples.
Higher mRNA expression in siGRK6 samples.
Merging the identified genes
Identification top hit candidate genes.
Pathway analysis.
B
TCGA Lung Adenocarcinoma (IlluminaHiSeq)
High GRK6
Low GRK6
FDR < 0.05
Significant mRNAs
n=17
n=26
Samples
C
RNASeq
Control
siGRK6
FDR < 0.05
Significant genes
n=3
n=3
Samples

Figure 3

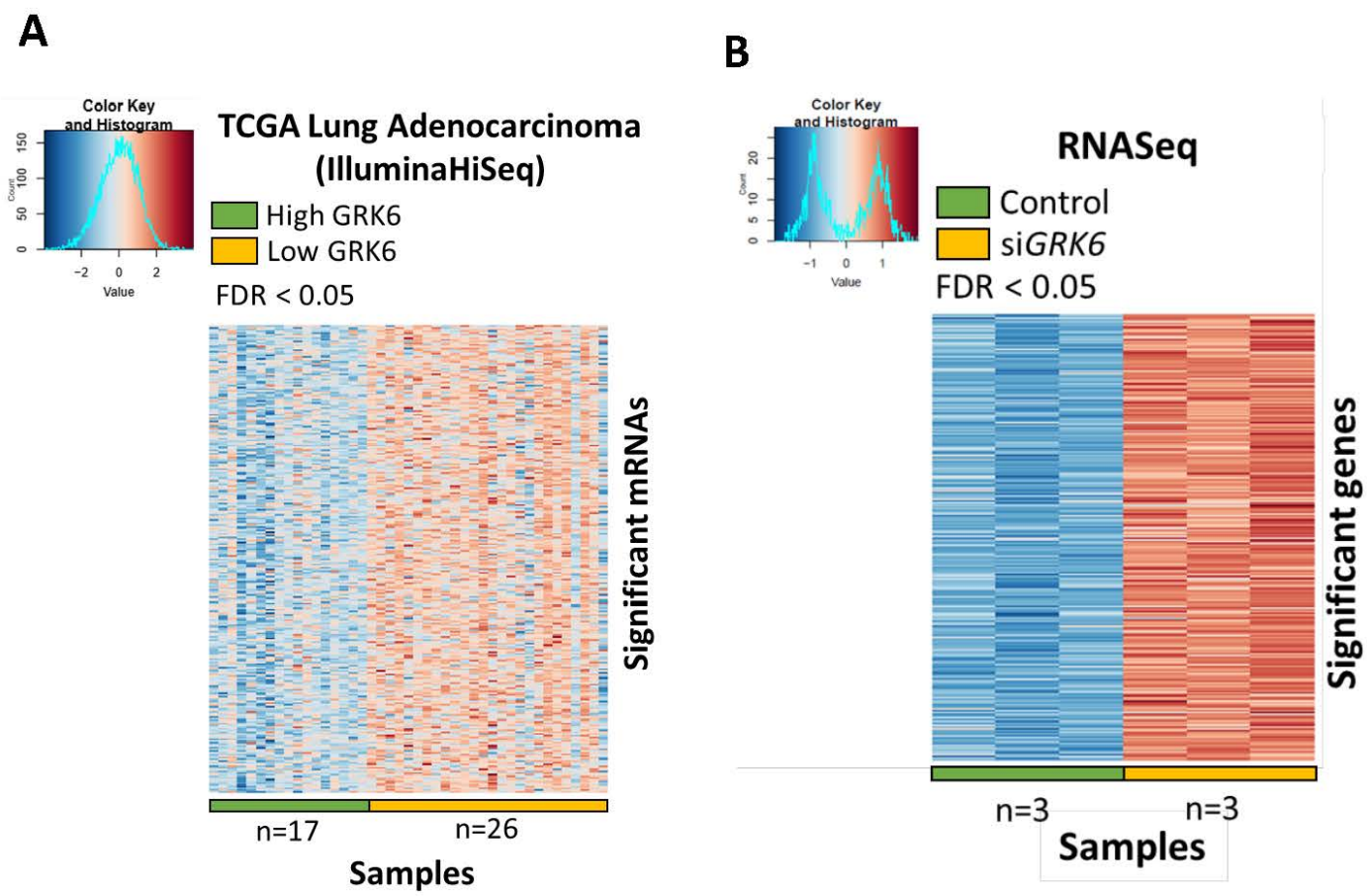
A
Color Key and Histogram
TCGA Lung Adenocarcinoma (IlluminaHiSeq)
High GRK6
Low GRK6
FDR < 0.05
Significant mRNAs
n=17
n=26
Samples
B
Color Key and Histogram
RNASeq
Control
siGRK6
FDR < 0.05
Significant genes
n=3
n=3
Samples

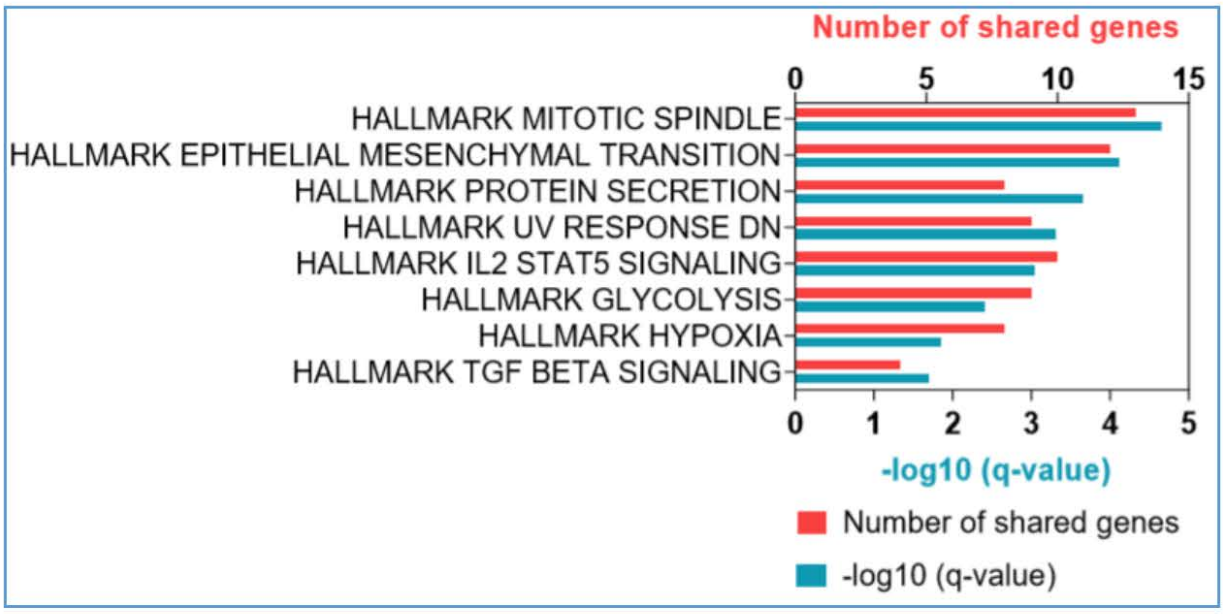
C
Number of shared genes
HALLMARK MITOTIC SPINDLE
HALLMARK EPITHELIAL MESENCHYMAL TRANSITION
HALLMARK PROTEIN SECRETION
HALLMARK UV RESPONSE DN
HALLMARK IL2 STAT5 SIGNALING
HALLMARK GLYCOLYSIS
HALLMARK HYPOXIA
HALLMARK TGF BETA SIGNALING
-log10 (q-value)
Number of shared genes
-log10 (q-value)

Figure 4

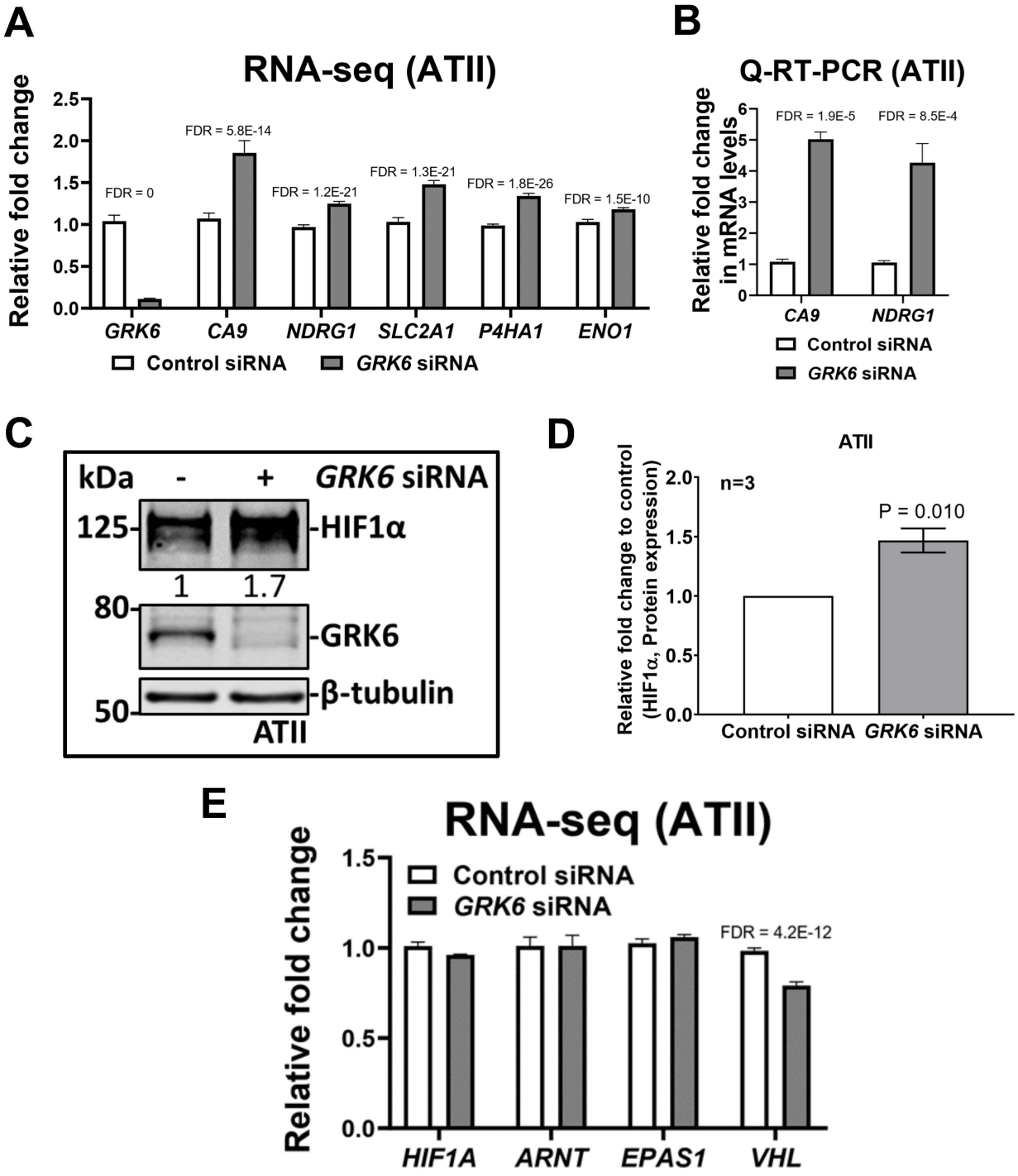
A
RNA-seq (ATII)
Relative fold change
FDR = 0
FDR = 5.8E-14
FDR = 1.2E-21
FDR = 1.3E-21
FDR = 1.8E-26
FDR = 1.5E-10
GRK6
CA9
NDRG1
SLC2A1
P4HA1
ENO1
Control siRNA
GRK6 siRNA
B
Q-RT-PCR (ATII)
Relative fold change in mRNA levels
FDR = 1.9E-5
FDR = 8.5E-4
CA9
NDRG1
Control siRNA
GRK6 siRNA
C
kDa
-
+
GRK6 siRNA
125
HIF1α
1
1.7
80
GRK6
50
β-tubulin
ATII
D
ATII
n=3
P = 0.010
Relative fold change to control (HIF1α, Protein expression)
Control siRNA
GRK6 siRNA
E
RNA-seq (ATII)
Relative fold change
Control siRNA
GRK6 siRNA
FDR = 4.2E-12
HIF1A
ARNT
EPAS1
VHL

Figure 5

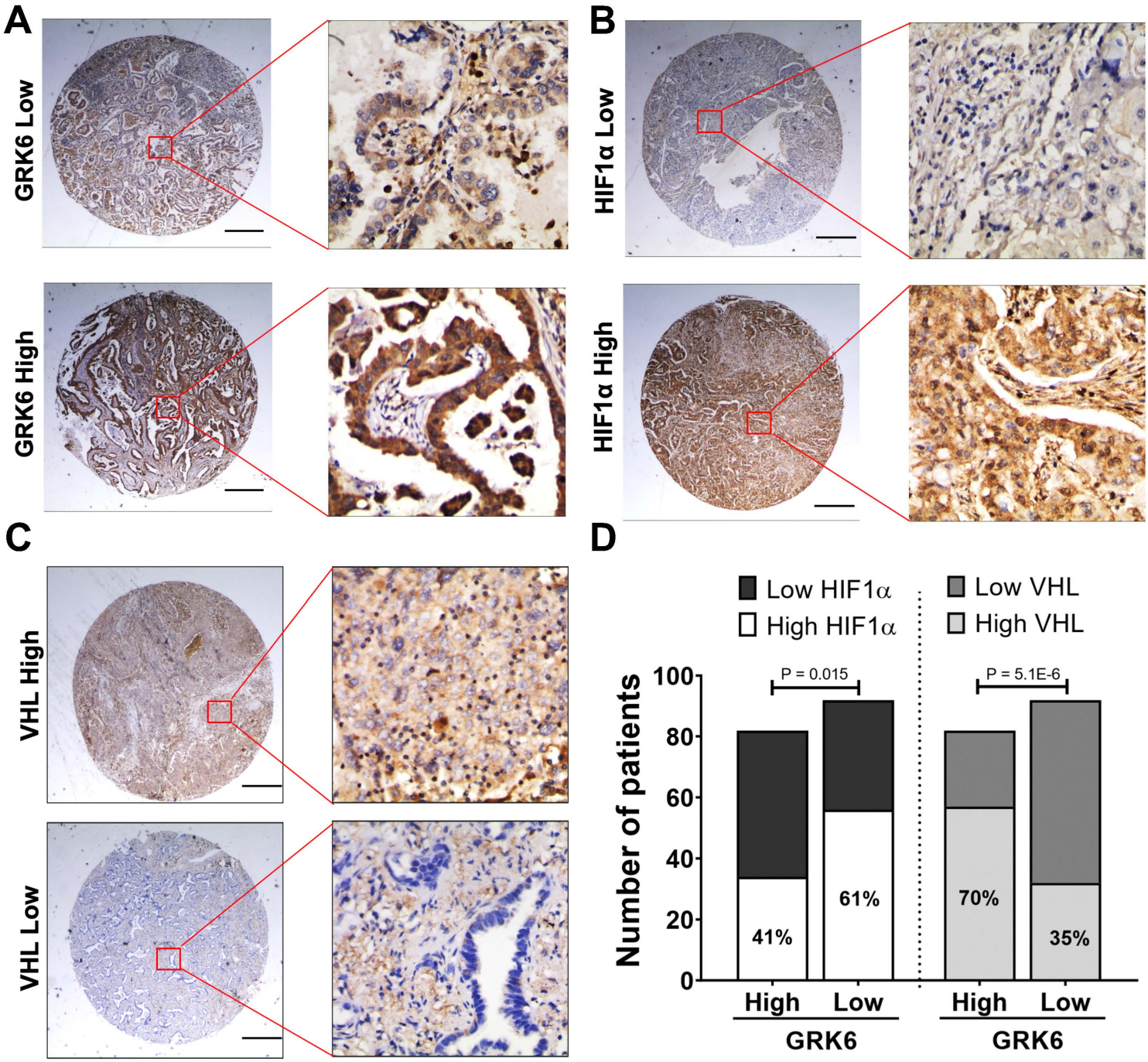
A
GRK6 Low
GRK6 High
B
HIF1α Low
HIF1α High
C
VHL High
VHL Low
D
Low HIF1α
High HIF1α
Low VHL
High VHL
P = 0.015
P = 5.1E-6
Number of patients
100
80
60
40
20
0
41%
61%
70%
35%
High
Low
High
Low
GRK6
GRK6

Supplementary Material

1 Supplementary Tables

1.1 Supplementary Table 1 Up-regulated DEGs in ATII cells transfected with siRNA against *GRK6 vs.* control siRNA.

1.2 Supplementary Table 2 Down-regulated DEGs in ATII cells transfected with siRNA against *GRK6 vs.* control siRNA.

1.3 Supplementary Table 3 GO analysis of up-regulated DEGs in ATII cells transfected with siRNA against *GRK6 vs.* control siRNA**.**

1.4 Supplementary Table 4 GO analysis of down-regulated DEGs in ATII cells transfected with siRNA against *GRK6 vs.* control siRNA.

1.5 Supplementary Table 5 List of candidate genes that are over-expressed in lung adenocarcinoma samples with low GRK6 compared to those with high GRK6 from TCGA analysis.

1.6 Supplementary Table 6 List of candidate genes that are over-expressed in ATII cells transfected with siRNA against *GRK6* (si*GRK6*) *vs.* control siRNA.

2 Supplementary Figures

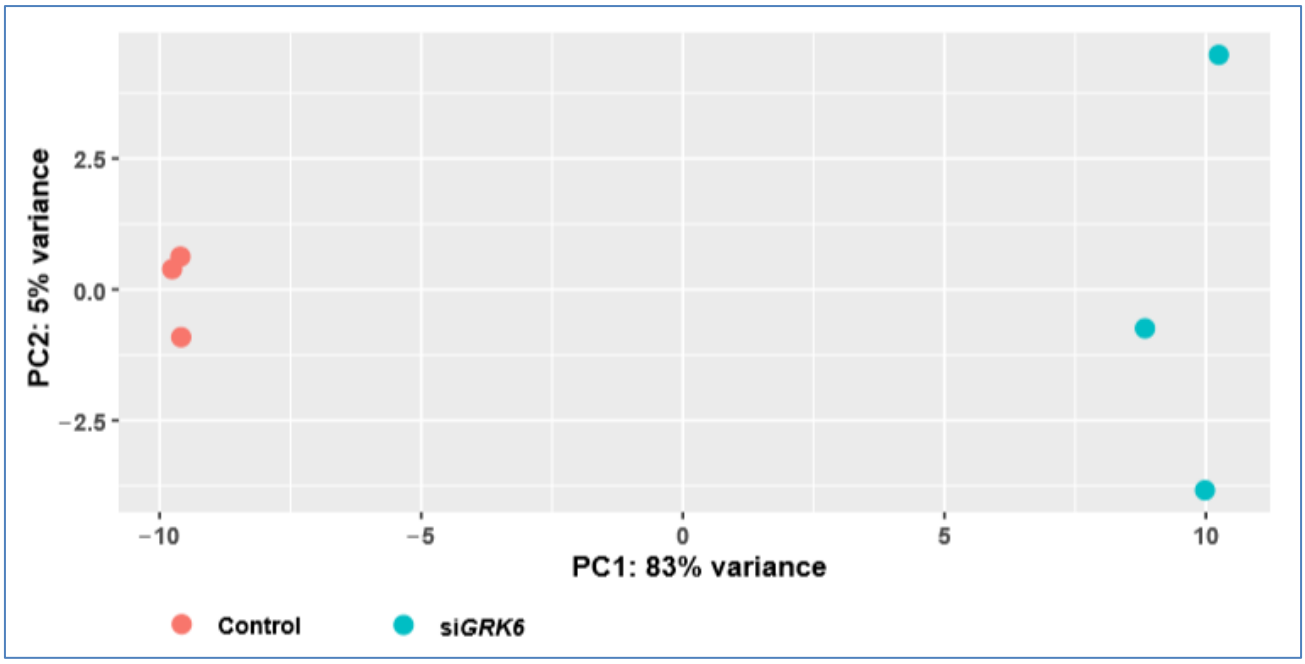

Supplementary Figure 1. Principal component analysis (PCA) between control and si*GRK6* samples from RNA-Seq data. ATII cells were transfected with control siRNA (Control, in red) or siRNA against *GRK6* (si*GRK6*, in blue) for 3 days, followed by RNA-Seq analysis. Each point represents an RNA-Seq sample. Samples that have similar gene expression patterns are clustered together.

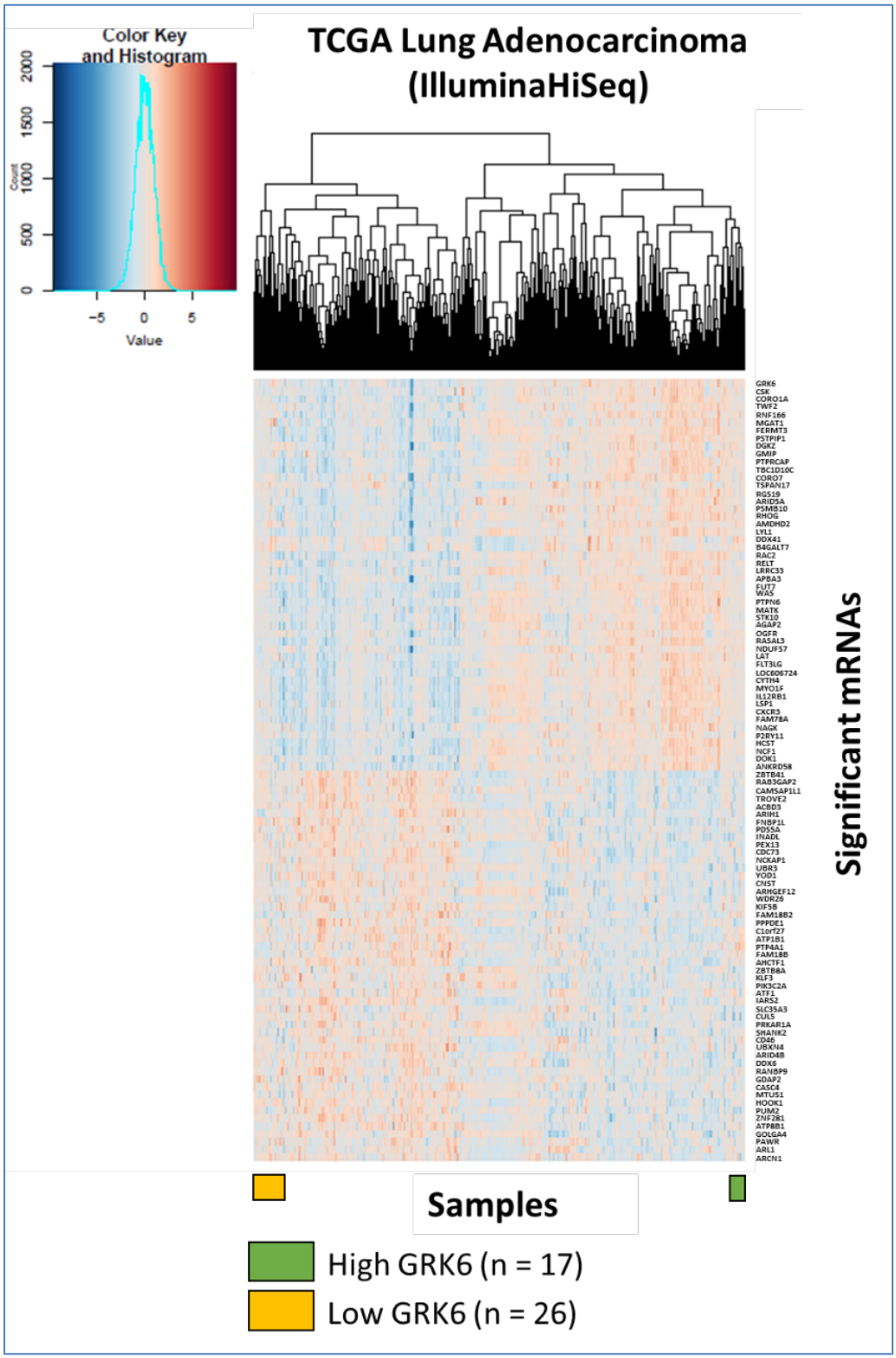

Supplementary Figure 2. Lung adenocarcinoma samples with either low or high GRK6 are identified in TCGA by unsupervised hierarchical clustering. Heat-map showing genes that are positively or negatively correlated with GRK6 expression levels in TCGA lung adenocarcinoma samples. A total of 17 samples were identified as high GRK6 (green box) and 26 as low GRK6 (yellow box). Red in heatmap indicates up-regulation and blue down-regulation.